

Evaluation of an Algebraic Technique for Colorimetric Calibration of a Printing System

Yoshihiko Azuma and Mitsuo Kaji[▲]

Department of Image Information Engineering, Tokyo Institute of Polytechnics, Atsugi-shi, Kanagawa, Japan

Shoji Otake

Kodak Polychrome Graphics Japan Ltd., Tokyo, Japan

J. S. Arney[▲]

Center for Imaging Science, Rochester Institute of Technology, Rochester, New York

A method is described for calibrating a trichromatic halftone printing system in CIELAB colorimetric coordinates. The calibration method involves the use of three analytic equations rather than a LUT and interpolations. Calibration is done empirically by sending to the printing system a set of dot fraction vectors, [c m y]. CIELAB [L*a*b*] vectors are measured for each printed sample, and a statistical and algebraic analysis then leads to three algebraic equations for converting [L*a*b*] vectors to [c m y] vectors. The quality and efficiency of this calibration technique are discussed in comparison to the more common LUT technique with interpolations. Calibration quality was measured both as the average and the maximum value of CIELAB ΔE between the printed and the calculated [L*a*b*] vectors. The potential utility of the algebraic method of calibration is discussed in terms of the tradeoff between colorimetric accuracy, computational speed, and the ease of performing the calibration.

Journal of Imaging Science and Technology 45: 93–99 (2001)

Introduction

The concept of device independent color (DIC) involves the use of a standard coordinate system for transmission of colorimetric information between imaging devices so that the color reproduced by any calibrated device can match the original image or any other calibrated device within the gamut limits of the device.¹ One such DIC is the CIELAB space represented by the color vector [L*a*b*]. In the current work, we have chosen [L*a*b*] as a representative DIC and have explored the efficiency and quality of an empirical calibration technique to convert [L*a*b*] into device dependent coordinates [c m y], where the c, m, and y represent the dot area fractions of a halftone printing system. Printing systems are often calibrated by developing a three-dimensional lookup table, LUT, to relate a set of, for example, [L*a*b*] values to a corresponding set of [c m y] values. The LUT is then used with an interpolation routine to convert any given [L*a*b*] into the [c m y] required to print it that particular color. In this kind of calibration, there is a clear correlation between the number of elements in the LUT and the accuracy of the calibration.^{2–4}

Alternative approaches to printer calibration based on physical models of printer behavior also have been suggested.^{5,6} These models are attempts to describe the effects of paper and ink physical and optical effects coupled with a description of the geometry of halftones. However, these models are generally designed to describe the output of a printer, [L*a*b*], as a function of the input [c m y]. A practical printer calibration requires the inverse operation of predicting [c m y] given the desired [L*a*b*], and physical models generally do not lead to invertible functions. Thus, practical printer calibrations still require an empirical LUT with interpolation.

In the current work, we explore an alternative to the LUT approach for printer calibration. This approach involves the development of an empirical, analytic expression for algebraically calculating [c m y] directly from [L*a*b*]. A technique for performing this calibration is given in this report, and the results are discussed in terms of colorimetric accuracy, the ease of carrying out the calibration, and the computational intensity of using the calibration in a printer. The algebraic calibration technique described in this report is based on similar work reported by Kunishi and Hioki.⁷ The results of this analysis are not meant to show one technique to be superior to another but to provide a detailed illustration of the analytical technique of calibration and to offer discussion relevant to the evaluation of calibration technique.

Original manuscript received April 6, 1999

▲ IS&T Member

Color Plate 1 is printed in the color plate section of this issue, p. 161.

©2001, IS&T—The Society for Imaging Science and Technology

Experimental

Test Target

Input [c m y K] values for the calibration were selected from the Standard Color Image Data (SCID), ISO12640.⁸ This data set contains 928 sets of [c m y K] vectors defined in ISO12642,⁹ which nominally form the test target shown in **Color Plate 1 (p. 161)**. All 928 vectors of [c m y K] were sent to the printing system. In order to simulate a natural printing condition, four natural image data sets, included in ISO/JIS-SCID CD-ROM, N1, N3, N4, and N7, were also sent to the printing system. Of the 928 printed test patches, 216 contain zero dot area fraction for the black ink, $K = 0$. These 216 patches consist of a set of only c, m, and y dot fractions, each with a value of 0, 0.1, 0.2, 0.4, 0.7, or 1.0. These six values in all possible combinations constituted the $6^3 = 216$ test vectors used in this study to calibrate the printer. This set of dot fractions was selected because it covers all values 0 to 1 but places more emphasis on the highlights where greater color calibration accuracy is desired.

Printing System

The printing system to which the [c m y] vectors were sent consisted of a Dainippon Screen image setter MTR-1120 with a Dainippon Screen KF-123-GL proof-printing machine. The image setter produced cm y color separation films with 175 lpi, square, clustered dot halftones. The films were used to expose the plate material, FPP-J made by Fuji Photo Film. Exposure of the plate was adjusted to reproduce the 8 μm lines in a Burner Chart. The KF-123-GL printing machine was operated in accord with JAPAN COLOR Condition,¹⁰ based on ISO12647-2,¹¹ which specifies the colorimetric values of the primary and secondary colors (RGBCMY) reproduced on a standard paper with standard inks specified in ISO2846.¹² Tokubishi-Art Paper of 128g/m² and JAPAN COLOR ink SF-90 were used. A Barcan New 278 blanket was used in the printer, and printing was done in the sequence CMYK.

Dot gain values of the printed halftone dots were measured as the difference between the dot area on the films, F_f , and that on the printed samples, F_o . Both F_f and F_o were estimated from transmission density and reflection density measurements respectively, and the density values were applied to the Murray–Davies equation, Eq. 1.

$$F = 100 \cdot \left[\frac{10^{-D_p} - 10^{-D_t}}{10^{-D_p} - 10^{-D_s}} \right] \quad (1)$$

In this equation, D_s is the density of the halftone tint at some value of F , D_s is the density at $F = 100$, and D_p is the density at $F = 0$. Dot gain values of the samples printed with the system described above were confirmed to be in accordance with ISO12647-2.

Measurement

All color measurements were conducted with the X-Rite938 spectrodensitometer and conform to ISO 13655¹³ with a 2° standard observer, D50 illuminant, a black backing, and a geometry of 45/0 or 0/45. All 928 printed color patches were measured, but only the 216 color patches with $K = 0$ were used in the current study.

Results

Distribution of Colorimetric Values

Figure 1(a) shows the distribution of points in $L^*a^*b^*$ space for the 216 printed test patches with the color

space set at 80 degrees to the a^* axis in the counter-clockwise direction. Note that all of the samples labeled at 70% cyan fall along a straight line. In fact, all of the samples occupy approximately the same plane in $L^*a^*b^*$ space and appear to form a straight line when projected in the 80 degree direction. Similarly, each set of points at any other fixed value of c also falls approximately on a unique plane. In other words, regardless of the values of m and y, all samples of the same value of c fall on the same plane.

Figures 1(b) and 1(c) show the same data from two additional perspectives, and it is evident that the magenta and yellow dot area fractions behave similarly to the cyan. Regardless of the values of c and y, all samples of the same value of m fall on the same plane, and regardless of the values of c and m, all samples of the same value of y fall on the same plane. This phenomenon of intersecting planes is not a property to be expected from all printing systems, but it does simplify the process of developing empirical algebraic equations for printer calibration. For a plane defined by a given value of c, we can write a linear equation with two slope terms and an intercept term as shown in Eq. 2.

$$L^* = \alpha a^* + \beta b^* + \gamma \quad (2)$$

The slope and intercept terms α , β , and γ are functions only of dot fraction c and not of m or y. Equations identical in form Eq. 2 can be written for the planes defined by m and for the planes defined by y. In each case, the slope and intercept terms, are functions only of either m or y. The significance of these equations is that they isolate the effects of the individual input channels [c m y] on the output [$L^*a^*b^*$]. Determination of these isolated c, m, and y functions is the major key to the calibration process.

Testing the Utility of the Planar Model

For each value of c in the project, a linear regression was performed to determine the values of α , β , and γ . Similarly, regression analysis determined the values of α , β , and γ for each value of m and for each value of y. Table I shows the result of all of the regressions. In order to verify the utility of the planar equation Eq. 2, the measured values of L^* for each of the 216 data points were compared to values of L^* calculated with Eq. 2 using the values of a^* and b^* with the regression values of α , β , and γ for cyan. The results are shown in Fig. 2(a). Similarly, Figs. 2(b) and 2(c) show the analysis for the magenta and the yellow. These correlations indicate the efficacy of the planar model. A number of metrics of efficacy might be used. The one chosen here was ΔL^* defined as the mean difference between the measured and calculated values of L^* . Values of $\Delta L^* = 1.16$, 1.93, and 0.87 were found of the cyan, magenta, and yellow planes respectively.

Determining the α , β , and γ Functions

The values of α , β , and γ were each plotted versus the value of c as shown in Fig. 3(a), and quadratic regression analyses resulted in the lines fit through the data points. The equations for these three functions can be written as shown in Eq. 3.

$$\begin{aligned} \alpha &= p_1 c^2 + q_1 c + r_1 \\ \beta &= p_2 c^2 + q_2 c + r_2 \\ \gamma &= p_3 c^2 + q_3 c + r_3 \end{aligned} \quad (3)$$

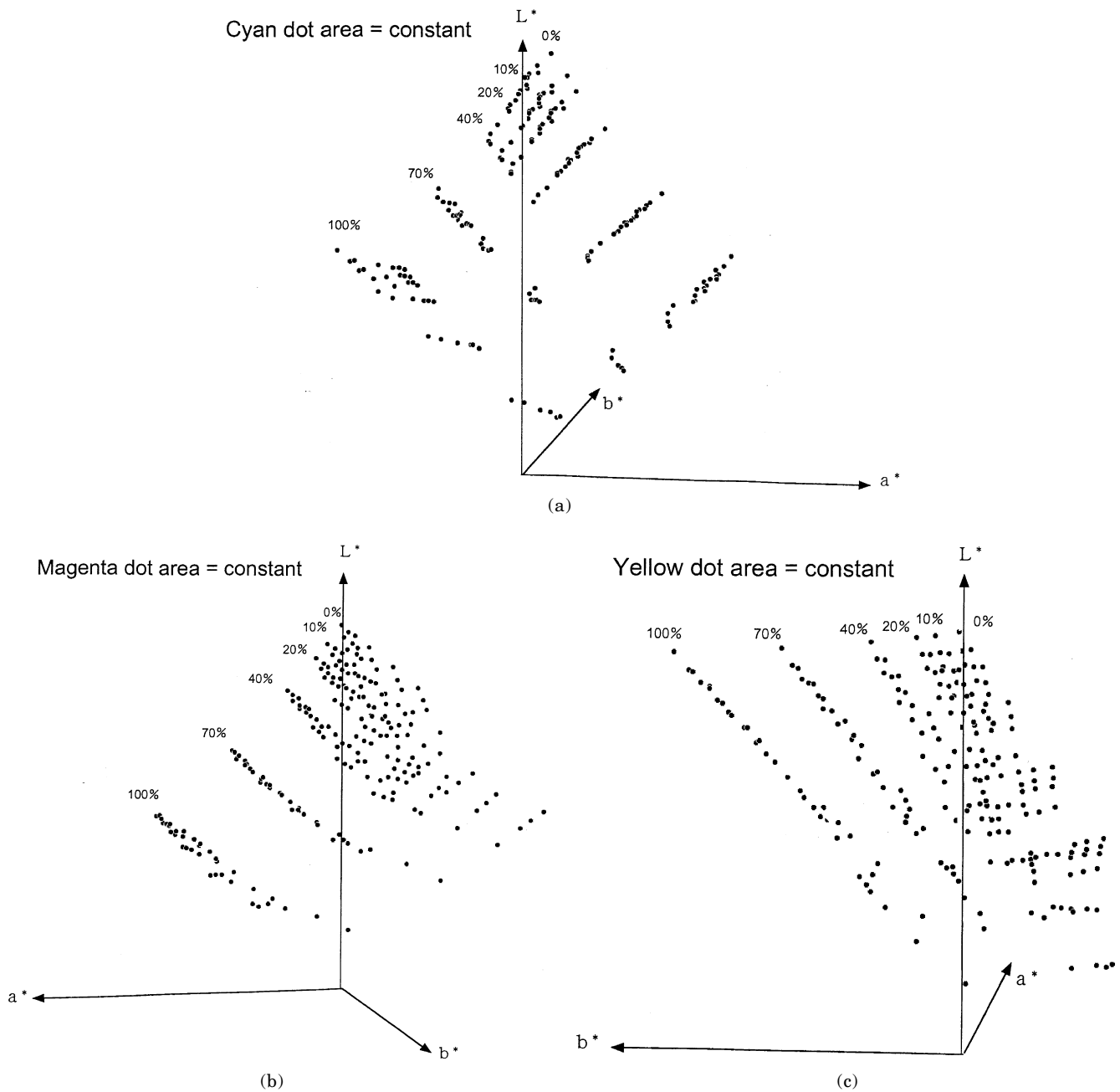


Figure 1. Views of plotted points of colorimetric values for all color patches in $L^*a^*b^*$ color space when viewed (a) at an angle of 80 degrees, (b) at an angle of 255 degrees, and (c) at an angle of 5 degrees, to the a^* -axis in the counterclockwise direction.

The values of p , q , and r ($i = 1, 2$ or 3) are constants characteristic of the printing system and are independent of c , m , and y . Table II shows the values of these constants determined by regression analysis of the data shown in Fig. 3(a). Figures 3(b) and 3(c) show the same analysis applied to the magenta and the yellow planes, and Table II shows the corresponding constants for Eq. 3 for the magenta and yellow planes.

It should be noted that quadratic equations were used to fit the data rather than higher order polynomials because an analytic inverse is needed for the printer calibration, as shown subsequently. The results in Fig. 3 clearly show the quadratic functions fit the data quite well enough relative to the magnitude of the error intrinsic to the planar model.

Building the Calibration Equation

By combining Eq. 3 with Eq. 2, the following quadratic equation results.

$$(p_1a^* + p_2b^* + p_3)c^2 + (q_1a^* + q_2b^* + q_3)c + (r_1a^* + r_2b^* + r_3 - L^*)c = 0 \quad (4)$$

This equation provides a unique relationship between c and the color coordinates L^* , a^* , and b^* . Thus, Eq. 4 is analogous to an analytical densitometry function that isolates the effect of each input channel of a color imaging system. Moreover, Eq. 4 can be solved analytically for the cyan dot area fraction. The solution

TABLE I. Planar Equations for Color Patches that Contain a Specified Dot Area of Each Primary Color.

fractional dot area	planar equation	coefficient of determination
Cyan		
0.0	$L^* = -0.6361a^* - 0.0963b^* + 90.2127$	0.9914
0.1	$L^* = -0.6308a^* - 0.1074b^* + 84.6260$	0.9914
0.2	$L^* = -0.6269a^* - 0.1155b^* + 79.5063$	0.9909
0.4	$L^* = -0.6132a^* - 0.1411b^* + 67.6345$	0.9894
0.7	$L^* = -0.5902a^* - 0.2071b^* + 45.0058$	0.9882
1.0	$L^* = -0.5815a^* - 0.3618b^* + 12.4127$	0.9915
Magenta		
0.0	$L^* = 0.7338a^* + 0.0836b^* + 87.8813$	0.9426
0.1	$L^* = 0.6851a^* + 0.0646b^* + 80.7086$	0.9533
0.2	$L^* = 0.6470a^* + 0.0533b^* + 74.9726$	0.9560
0.4	$L^* = 0.5516a^* + 0.0306b^* + 62.6850$	0.9660
0.7	$L^* = 0.4533a^* + 0.0171b^* + 41.2061$	0.9737
1.0	$L^* = 0.4288a^* + 0.0745b^* + 14.8254$	0.9764
Yellow		
0.0	$L^* = -0.6133a^* + 1.2606b^* + 93.1936$	0.9944
0.1	$L^* = -0.5215a^* + 1.1376b^* + 82.7483$	0.9947
0.2	$L^* = -0.4823a^* + 1.0945b^* + 76.1408$	0.9948
0.4	$L^* = -0.3740a^* + 1.0033b^* + 60.6783$	0.9956
0.7	$L^* = -0.2357a^* + 0.8683b^* + 38.0032$	0.9965
1.0	$L^* = -0.1484a^* + 0.7332b^* + 18.8033$	0.9971

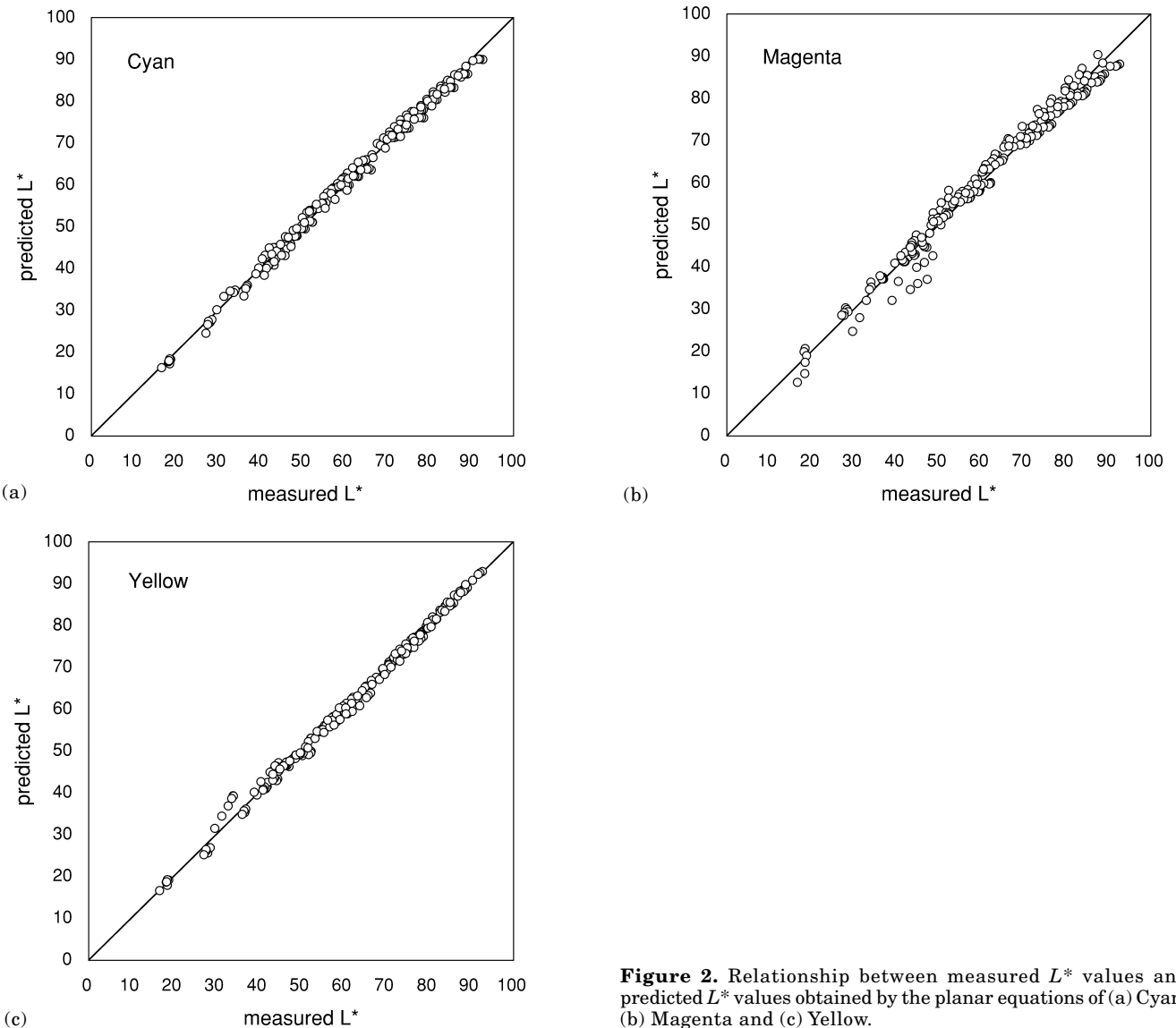


Figure 2. Relationship between measured L^* values and predicted L^* values obtained by the planar equations of (a) Cyan, (b) Magenta and (c) Yellow.

TABLE II. Coefficient Values of Quadratic Equations that Represent α , β , and γ as Functions of Dot Area of Each Primary Color.

Coefficient	p_i	q_i	r_i
Cyan			
α	-0.0142	0.0723	-0.6380
β	-0.2899	0.0379	-0.1046
γ	-38.404	-38.053	89.335
Magenta			
α	0.2655	-0.5819	0.7408
β	0.2311	-0.2482	0.0878
γ	-18.213	-53.646	86.998
Yellow			
α	-0.2219	0.6781	-0.6042
β	0.1634	-0.6544	1.2317
γ	12.055	-85.837	92.514

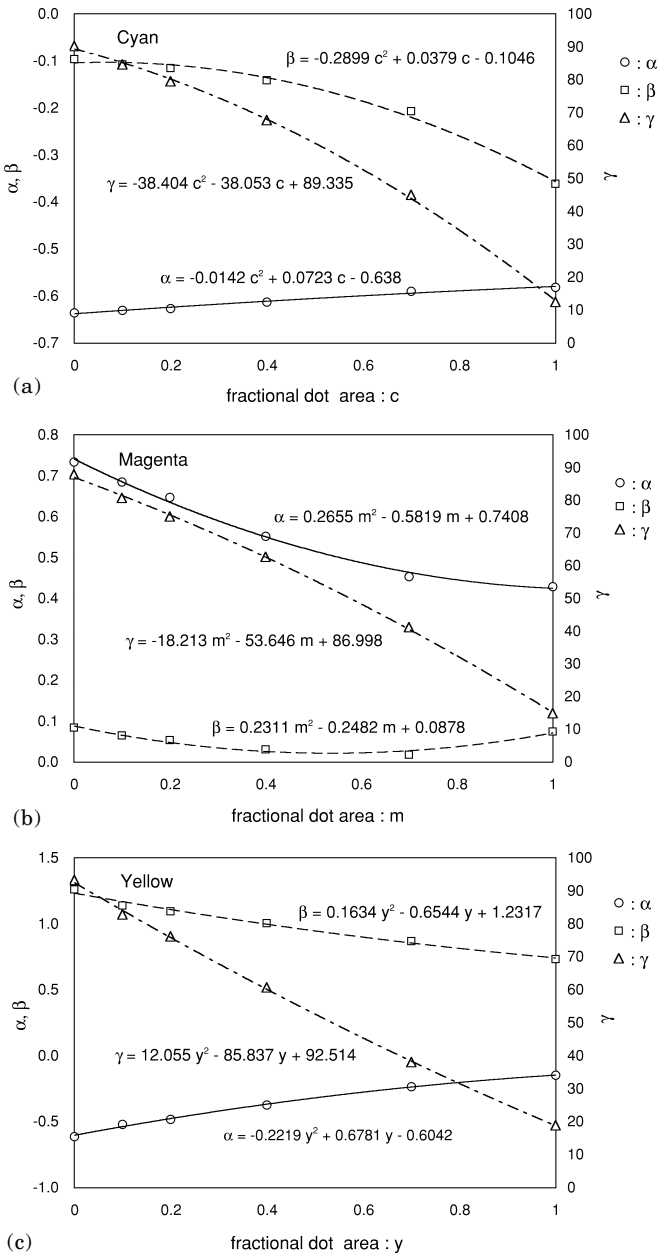


Figure 3. Relationship between fractional dot areas and coefficient values of the planar equations of (a) Cyan, (b) Magenta and (c) Yellow.

to a quadratic equation can produce two solutions, but only one provides a physically meaningful solution with $c \geq 0$. That solution is shown as Eq. 5,

$$c = \frac{-B - \sqrt{B^2 - 4AC}}{2A} \quad (5)$$

where

$$A = p_1a^* + p_2b^* + p_3 \quad (6)$$

$$B = q_1a^* + q_2b^* + q_3 \quad (7)$$

$$C = r_1a^* + r_2b^* + r_3 - L^* \quad (8)$$

Similar quadratic equations can be derived for the magenta and the yellow planes, and the results provide a direct calculation for the dot fractions, [c m y], needed to print any given color [L*a*b*].

Discussion

Gamut Limits

The question of out of gamut colors is always an issue with device independent color, and detection of out of gamut colors is essential to the practical application of any printer calibration. In the current example, out of gamut colors are easily detected when calculated values of c, m, and/or y fall outside the range 0 to 1. In the current analysis, out of gamut colors were simply assigned the limiting values of 0% or 100%. The strategy for dealing with such out of gamut colors is not within the scope of the current discussion.

A related problem occurs when $(B^2 - 4AC) < 0$. This results in a complex solution for Eq. 5. This situation is quite rare and occurred only with three of the 216 samples in the current analysis. These three samples were excluded from the remainder of the analysis.

Accuracy

The accuracy of the printer calibration in the current experiment was measured by applying the analytical equations of Eq. 5 to the 213 sets of [L*a*b*] measured for the printed samples. The resulting [c m y] values were then compared to the original [c m y] values that had been sent to the printer to print the samples. Figure 4(a) illustrates the results for the 36 samples for $c = 0$. Some of the samples exceeded the dot fraction limits of 0 and 100%, and Fig. 4(b) shows the data truncated to maintain these limits. The differences between the dot fractions sent to the printing system and the values calculated from Eq. 5, with gamut limiting, were calculated. Average differences of 1.6%, 2.8%, and 1.2% were calculated for cyan, magenta, and yellow respectively, with corresponding maximum values of 5.7%, 20.0%, and 9.8%.

The accuracy of the calibration can also be examined in L*a*b* space. This was achieved by recognizing that Eq. 4 can be written for cyan, magenta, and yellow, resulting in three simultaneous equations. Solving the three equations leads to three different equations, one for calculating L*, one for a*, and one for b*. Each new equation is a function of [c m y]. The original values of [c m y] that were sent to the printer were used to calculate the values of [L*a*b*] that should have been printed if the calibration were perfectly accurate. These values of [L*a*b*] were compared to the [L*a*b*] values measured for the actual printed samples. The differences represented as ΔE_{ab}^* for the 213 samples in the study are shown in Fig. 5. The average color difference was 3.01 with a maximum of 11.9.

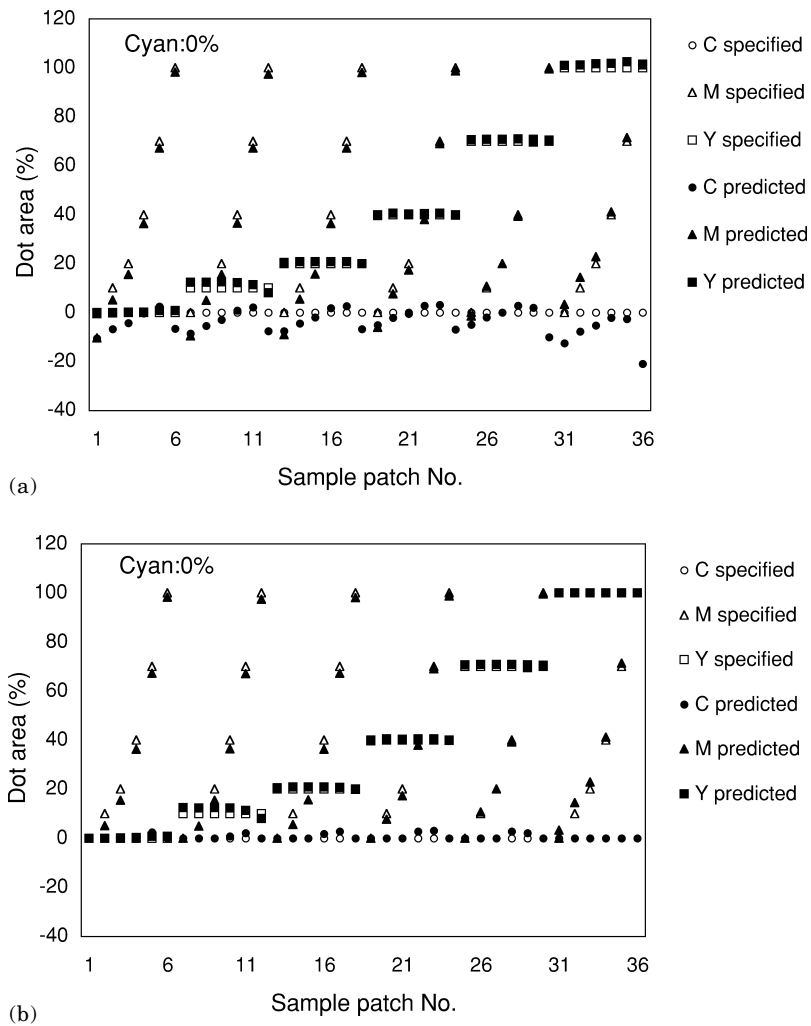


Figure 4. Comparison of calculated dot areas with specified dot areas when c (fractional dot area of C primary) = 0.0, (a) before limiting, and (b) after limiting.

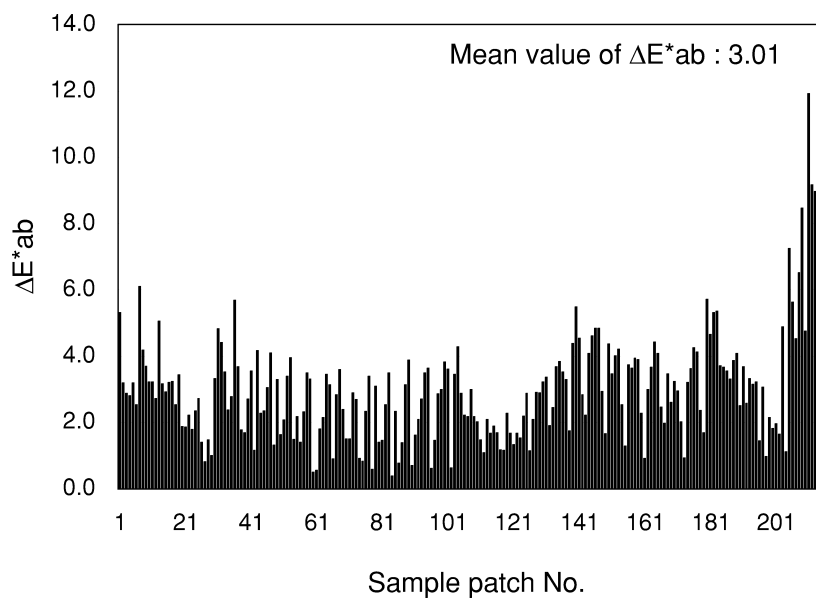


Figure 5. Color differences between calculated $L^*a^*b^*$ values and measured $L^*a^*b^*$ values for 213 color patches.

TABLE III. Comparison of Computation Time in Seconds Between the Proposed Method and the LUT Interpolation Method.

	LUT Interpolation method			Proposed method
	5 ³	9 ³	17 ³	
Number of lattice points	5 ³	9 ³	17 ³	—
Computation time	8.5	51.3	389.4	1.3

Computation Speed

A comparison was made between the CPU computation times required by the algebraic method of calibration with Eq. 5 and the LUT interpolation method for converting a set of $[L^*a^*b^*]$ to $[c\ m\ y]$. The tetrahedral interpolation method was chosen for this comparison as a representative technique often used for conversion from a distorted space such as $[L^*a^*b^*]$ to a cubic space such as $[c\ m\ y]$. Usually, a reshaping of the distorted space is performed prior to such conversion, but was not used in this comparison.

Three LUTs for the comparison, whose size $n = 5, 9,$ and $17,$ were constructed from different data sets of $[c\ m\ y]$ and $[L^*a^*b^*]$. The data set used in each LUT was generated by dividing $[c\ m\ y]$ space into n^3 equally spaced lattice points and by calculating the corresponding $[L^*a^*b^*]$ points based on a simple Neugebauer model.

A computational comparison was performed for 33^3 test points. These test points were set in the same way as the LUT lattice points. Color accuracy between the 33^3 sets of $[c\ m\ y]$ and $[L^*a^*b^*]$ was not of importance in this test, but the simulated data set was suitable for measuring computation time.

Computation time was measured by programming Eq. 5 in Microsoft Visual C++ (ver.6.0) running on a PC with Windows NT (ver.4.0), 128 MB IC memory, an Intel Celeron CPU at 466 MHz, and a 10 GB hard drive. The time required to convert the 33^3 $[L^*a^*b^*]$ points to $[c\ m\ y]$ was measured as 1.3 seconds. The LUT interpolation program was also programmed and run in this system, and the time required to perform the 33^3 $[L^*a^*b^*]$ points to $[c\ m\ y]$ conversions using 5³-LUT was 8.5 seconds. Computation times were measured in this way also for 9³-LUT and for 17³-LUT, and the results are shown in Table III. The results indicate the LUT interpolation technique can require orders of magnitude more time to process than the algebraic method.

Conclusions

Choosing a calibration technique for a given printing application is complex process requiring consideration of many factors. The work reported here was performed as a means of exploring some of these factors for the analytic algebraic method of calibration. The authors suggest that the algebraic method of calibration may have several attributes that may make it the method of choice in some applications.

Color accuracy is always a factor in considering a printer calibration technique, and the level of accuracy observed in this example of the algebraic technique is clearly sufficient for many practical applications. Any desired level of accuracy can be achieved with a LUT technique simply by adding more calibration points to the LUT. The accuracy of the algebraic calibration can be expected to be much less sensitive to changes in the

number of calibration data points. Beyond a few tens or hundreds of calibration points, the level of accuracy is a function more of the accuracy of the algebraic model than the accuracy or number of calibration data points. The accuracy of the algebraic model depends on knowledge of the behavior of the printer and may be expected to improve as more research leads to greater understanding of printing processes.

The low sensitivity of the algebraic method to changes in the number of calibration points may provide a very useful advantage over LUT calibrations when the number of calibration points is limited. For example, in cases where the printing operator is required to perform the printer calibration, the algebraic method may require printing and measurement of significantly fewer samples compared to LUT techniques for a given level of color accuracy in the operation of the printing process.

Computational intensity is a complex factor and is difficult to generalize since so many computation environments may be applied to a given problem. The overall need is to have the computation time for an $[L^*a^*b^*]$ to $[c\ m\ y]$ conversion be negligible relative to the throughput rate required of the printing system. For a desk top printing operation that depends on a PC for the calibration operation, as illustrated above, the computation time required for the LUT interpolation method can be excessive relative to calibration with Eq. 5. The computational advantages and disadvantages for any given method of calibration must be evaluated individually for any chosen printing system.

In conclusion, the authors recommend the algebraic method of calibration for considered as a potentially viable method of calibration in many printing applications. Additional work is planned by the authors for continued exploration of this technique. ▲

Acknowledgment. Authors would like to express their grateful appreciation to students Hideo Tanaka, Kouichi Ito, and Kentaro Nozaki for their technical assistance.

Reference

1. International Color Consortium Profile Format Specification, Version 3.2, anonymous FTP: <ftp://sgigate.sgi.com/pub/icc/ICC34.pdf> (1997).
2. Po-Chieh Hung, Colorimetric calibration in electronic imaging devices using a look-up-table model and interpolations, *J. Electron. Imag.* **2**, 53 (1993).
3. J. M. Kasson, Tetrahedral interpolation algorithm accuracy, *Proc. SPIE* **2170**, 24 (1994).
4. H. R. Kang, Comparisons of three-dimensional interpolation techniques by simulations, *Proc. SPIE* **2414**, 104 (1995).
5. J. S. Arney, T. Wu and C. Blehm, Modeling the Yule-Nielsen Effect on Color Halftones, *J. Imaging Sci. Technol.* **42**, 335 (1998)
6. B. Kruse and M. Wedin, A New Approach to Dot Gain Modeling, *TAGA Proc.* 329 (1995)
7. T. Kunishi and R. Hioki, Study on the Offset Reproduction, *Bulletin of the Japanese Society of Printing Science and Technology*, **9**, 82 (1967).
8. ISO 12640:1997 Graphic technology—Prepress digital data exchange—CMYK standard color image data (CMYK/SCID).
9. ISO 12642:1996 Graphic technology—Prepress digital data exchange—Input data for characterization of 4-colour process printing.
10. M. Kaji, S. Otake and Y. Azuma, Colorimetric Characteristics of Process Color Prints Produced under the JAPAN COLOR Conditions, *Proc. IS&T's NIP 12 Conference*, IS&T, Springfield, VA, 1996, p. 94.
11. ISO 12647-2:1996 Graphic technology—Process control for the manufacture of halftone colour separations, proof and production prints—Part 2: Offset lithographic processes.
12. ISO 2846-1:1997 Graphic technology—Colour and transparency of ink sets for four-colour-printing—Part 1: Sheet-fed and heat-set web offset lithographic printing.
13. ISO 13655:1996 Graphic technology—Spectral measurement and colorimetric computation for graphic arts images.